Journal of the Taiwan Institute of Chemical Engineers xxx (xxxx) xxx

Contents lists available at ScienceDirect

Journal of the Taiwan Institute of Chemical Engineers

journal homepage: www.journals.elsevier.com/journal-of-the-taiwan-institute-of-chemical-engineers

$Na_5YSi_4O_{12}$-polymer composite coating for hard carbon: a strategy to improve sodium-ion storage performance

Mohamed M. Abdelaal [a,b], Pandeeswari Jayaraman [a], Kei Nishikawa [c], Masashi Kotobuki [a,d,*]

[a] Battery Research Center of Green Energy, Ming Chi University of Technology, Taiwan
[b] Tabbin Institute for Metallurgical Studies (TIMS), Egypt
[c] Research Center for Environmental Energy Science, National Institute for Materials Science, Japan
[d] Center for Sustainability and Energy Technologies, Chang Gung University, Taiwan

ARTICLE INFO

Keywords:
Na battery
Hard carbon
Conductive surface layer
Active filler
Cycling stability
Initial coulombic efficiency

ABSTRACT

Background: Hard carbon (HC) anodes demonstrate significant potential for sodium-ion batteries but suffer from low initial Coulombic efficiency (ICE) and poor cycling stability. To address these limitations, this study introduces a novel $Na_5YSi_4O_{12}$ (NYSO)-based composite coating, where NYSO particles are incorporated as conductive fillers within a PVdF-HFP matrix and applied onto HC particles for the first time.
Method: NYSO was synthesized via solid-state reaction and uniformly dispersed in a PVdF-HFP matrix containing $NaClO_4$. After optimizing the NYSO filler ratio, the composite was coated onto HC particles. The ionic conductivity and activation energy of both pure NYSO and the composite layer were systematically evaluated before electrochemical testing.
Significant findings: NYSO exhibited a total ionic conductivity of 1.3×10^{-4} S cm^{-1} at room temperature, while the composite layer achieved 4.6×10^{-5} Scm^{-1}. The coated HC anode demonstrated remarkable performance, with an ICE of 89 % (*vs.*85 % for bare HC) and exceptional cycling stability (~100 % capacity retention over 200 cycles at 200 mA g^{-1}). These results confirm the effectiveness of the NYSO-based coating in enhancing interfacial stability and sodiation kinetics.

1. Introduction

Sodium-ion batteries (SIBs) have emerged as a promising alternative to lithium-ion batteries due to the abundance and low cost of sodium resources. Among the various anode materials for SIBs, hard carbons (HCs) are considered one of the most realistic candidates due to their high capacity, dendrite-free nature, and ability to store sodium ions through multiple mechanisms, including intercalation, adsorption, and pore-filling [1–3]. Like graphite anode on lithium-ion batteries, HCs exhibit a plateau around at 0.001 V *vs.* Na/Na^+, providing a wider electrochemical working window and, consequently, high energy density [2,4]. These properties, along with the high abundance of raw materials, make HCs a promising choice for large-scale applications [3].

However, HCs have faced significant challenges, particularly their low initial Coulombic efficiency (ICE), typically around 80 % [3]. This is primarily due to the loss of sodium ions during the formation of the solid-electrolyte interface (SEI) and the filling of pores with electrolyte decomposition products [2,5]. While tuning the synthesis temperature or modifying the surface area of HCs can improve ICE, these approaches have often reduced the capacity [3]. For instance, Younesi et al. increased ICE from 69 % to 89 % by reducing the specific surface area of HCs, but this also limited their capacity [6]. For real-world applications, enhancing ICE is a key parameter, as it directly impacts the reversible capacity and long-term cycling stability.

Researchers have explored strategies to improve the electrochemical performance of HC, including the use of additives, pre-sodiation, and surface coatings [7–10]. Additives, such as fluoroethylene carbonate (FEC), have been widely studied for their ability to inhibit electrolyte decomposition and improve ICE by forming a stable and thin SEI [7]. Fang et al. achieved an ICE of nearly 100 % in a half-cell configuration by electrochemically pre-sodiating HCs using sodium biphenyl, demonstrating the potential of pre-sodiation to address irreversible sodium loss [8]. However, the complexity and inconsistent results of pre-sodiation processes remain significant barriers to their industrial adoption [8]. Surface coatings, acting as pre-SEI layers, also improve ICE and electrochemical performance of HCs [7].

* Corresponding author.
E-mail address: kotobuki@mail.mcut.edu.tw (M. Kotobuki).

https://doi.org/10.1016/j.jtice.2025.106329
Received 17 April 2025; Received in revised form 14 July 2025; Accepted 4 August 2025
1876-1070/© 2025 Taiwan Institute of Chemical Engineers. Published by Elsevier B.V. All rights are reserved, including those for text and data mining, AI training, and similar technologies.

Please cite this article as: Mohamed M. Abdelaal et al., *Journal of the Taiwan Institute of Chemical Engineers*, https://doi.org/10.1016/j.jtice.2025.106329

Despite these advancements, there is a pressing need to develop scalable and cost-effective solutions that simultaneously address the challenges of low ICE, capacity loss, and SEI instability in HCs [9,10]. Most existing approaches either require complex processes or fail to balance performance improvements with practical feasibility. For instance, while surface modifications and coatings have shown potential, many suffer from poor ionic conductivity or mechanical instability, limiting their applicability in battery systems. Therefore, there is a growing interest in designing composite coatings that combine high ionic conductivity, flexibility, and ease of fabrication to enable the widespread adoption of HCs in SIBs [11].

In this study, we propose a novel approach to enhance the performance of HCs by coating with a Na^+ conductive composite layer consisting of $Na_5YSi_4O_{12}$ (NYSO) filler dispersed in a poly(vinylidene fluoride-co-hexafluoropropylene) (PVdF-HFP) matrix. NYSO is a promising ceramic electrolyte with high Na^+ conductivity, however NYSO-based conductive composites have not been explored for HC modification. In this study, the NYSO-based conductive composite was applied for HC as a coating layer for the first time. This coating combines high Na^+ conductivity with flexibility, lowering interfacial resistance and improving electrochemical performance. Our results demonstrate that coated HCs exhibit higher ICE, high cyclability and enhanced SEI stability compared to bare HCs, offering a scalable solution for practical applications in sodium-ion batteries.

2. Experimental section

2.1. Synthesis of NYSO filler

NYSO (sodium yttrium silicate oxide, $Na_5YSi_4O_{12}$) was synthesized via a solid-state reaction using stoichiometric Na_2CO_3, Y_2O_3, and SiO_2 precursors [12]. The mixed powders were ball-milled in ethanol, dried at 80 °C, then calcined at 950 °C for 8 h. The product was re-milled, pressed into pellets (15.8 mm diameter, 10 MPa), and sintered at 1100 °C for 36 h to obtain dense, crystalline NYSO.

2.2. Preparation of composite coating layer

Composite membranes of PVdF-HFP:$NaClO_4$ (80:20 wt%.) were prepared with varying loadings (0∼10 wt %) of nano-sized NYSO, milled in absolute ethanol. These membranes are designated M-0 to M-10. The polymer was dissolved in DMF (60 °C, 300 rpm, 3 h), followed by $NaClO_4$ addition at 25 °C. NYSO filler was incorporated and stirred for 24 h. For characterization, free-standing membranes were prepared by doctor-blading onto glass and dried at 5 °C for 5 days. For preparation of coated HC electrodes, commercial hard carbon particles (Taiwan Carbon Materials Corp.) were uniformly coated with NYSO/PVDF-HFP composite (1 wt % coating mass). The slurry was homogenized by stirring at room temperature for 24 h, followed by controlled drying (5 °C for 5 days) and final vacuum drying (80 °C, 4 h) to obtain the coated hard carbon.

2.3. Structural and morphological characterization

The crystalline structures of NYSO, composite layer, bare HC (b-HC), and coated HC (c-HC) were analyzed by X-ray diffraction (XRD; Bruker D2 PHASER, Cu-Kα radiation, λ = 1.5406 Å, 30 kV, 10 mA). NYSO pellets were ground to a fine powder using an agate mortar to minimize preferred orientation of the XRD measurement. The morphology was examined by SEM (JSM-IT200, JEOL), with elemental composition determined by EDX and transmission electron microscopy (TEM, JEM-2100, JEOL Ltd.) operated at an accelerating voltage of 200 kV. The coating layer was characterized by XPS (PHI 5000 VersaProbe III, Al Kα radiation, λ = 8.3406 Å, 100 μm beam size).

2.4. Electrochemical experiments

Electrochemical impedance spectroscopy (EIS) was performed at room temperature with a 10 mV AC amplitude. The total ionic conductivity (σ_t) was calculated using Eq. (1) [13]:

$$\sigma_t = \frac{l}{RA} \tag{1}$$

where l is the thickness, R is the total real impedance, and A is the contact area between the blocking electrode and electrolyte. The activation energy (E_a) was determined applying the Arrhenius equation (Eq. (2)) [12,14]:

$$\sigma_t = A\exp(-E_a / RT) \tag{2}$$

where A is the pre-exponential factor, R is the universal gas constant (8.3 J K^{-1} mol^{-1}), and T represents absolute temperature in Kelvin.

For the preparation of the hard carbon electrode, a slurry was formulated with a weight ratio of 90:5:5 for the active material (b-HC or c-HC), Super P, and PVdF binder, respectively. The slurry was prepared using N-methyl-2-pyrrolidone (NMP) as the solvent to achieve the desired viscosity. The slurry was uniformly coated onto an aluminum foil current collector and dried at 60 °C for 24 h, followed by further drying at 120 °C for 1 hour to remove residual solvent. After calendaring, the electrode exhibited an active area of 1.33 cm^2, a thickness of approximately 30 μm, and a mass loading of ∼3 mg cm^{-2}.

Half-cells were assembled in an argon-filled glovebox (<0.5 ppm O_2 and H_2O) using sodium metal counter/reference electrode, a glass fiber separator (Whatman GF/D, 260 μm), and 1 M $NaPF_6$ in EC:DMC (1:1 *v/v*) electrolyte. Galvanostatic cycling (0.001–2.5 V *vs.* Na/Na^+) was performed on a NEWARE system. Cyclic voltammetry (0.2–10 mV sec^{-1}) assessed electrochemical behavior, with subsequent kinetic analysis differentiating diffusion-controlled and capacitive contributions. This analysis was conducted using Eq. (3) [15,16]:

$$i(v) = k_1 v + k_2 v^{1/2} \tag{3}$$

where $i(v)$ represents the total stored charge, $k_1 v$ corresponds to the surface-controlled capacitive contribution, and $k_2 v^{½}$ denotes the diffusion-controlled contribution, both expressed as functions of the scanning rate (v). The sodium-ion diffusion coefficient (D) was determined using the Randles-Sevcik equation (Eq. (4)) [9]:

$$i_p = \left(2.69 \times 10^5\right) \cdot n^{3/2} \cdot A \cdot D^{1/2} \cdot C \cdot v^{1/2} \tag{4}$$

where i_p is the peak current of the oxidation or reduction peaks, n is number of electrons transferred, A is the surface area, C is the concentration of sodium ions in the electrolyte, and v is the scan rate.

3. Results and discussion

3.1. Characterization of NYSO filler

XRD confirmed pure $Na_5YSi_4O_{12}$ synthesis (JCPDS# 32–1204) with no impurities (Fig. S1), exhibiting rhombohedral structure (*R*-3*c*) with sharp peaks indicating high crystallinity without the presence of secondary phases [12,17]. EDX mapping (Fig. S2) confirmed homogeneous element distribution, with measured composition (27.8 % Na, 3.6 % Y, 13.0 % Si, 55.6 % O) matching theoretical values (Fig. S3) [18]. EIS (Fig. S4a) revealed high ionic conductivity (1.3×10^{-4} S cm^{-1}) through equivalent circuit modeling (bulk resistance (R_b), grain boundary resistance (R_{gb}), and a constant phase element (Q) associated with surface charge adsorption) [19]. Arrhenius analysis (Fig. S4b) showed low activation energy (0.16 eV), enabling efficient ion transport across temperatures [20,21], making NYSO ideal for wide-range applications [12].

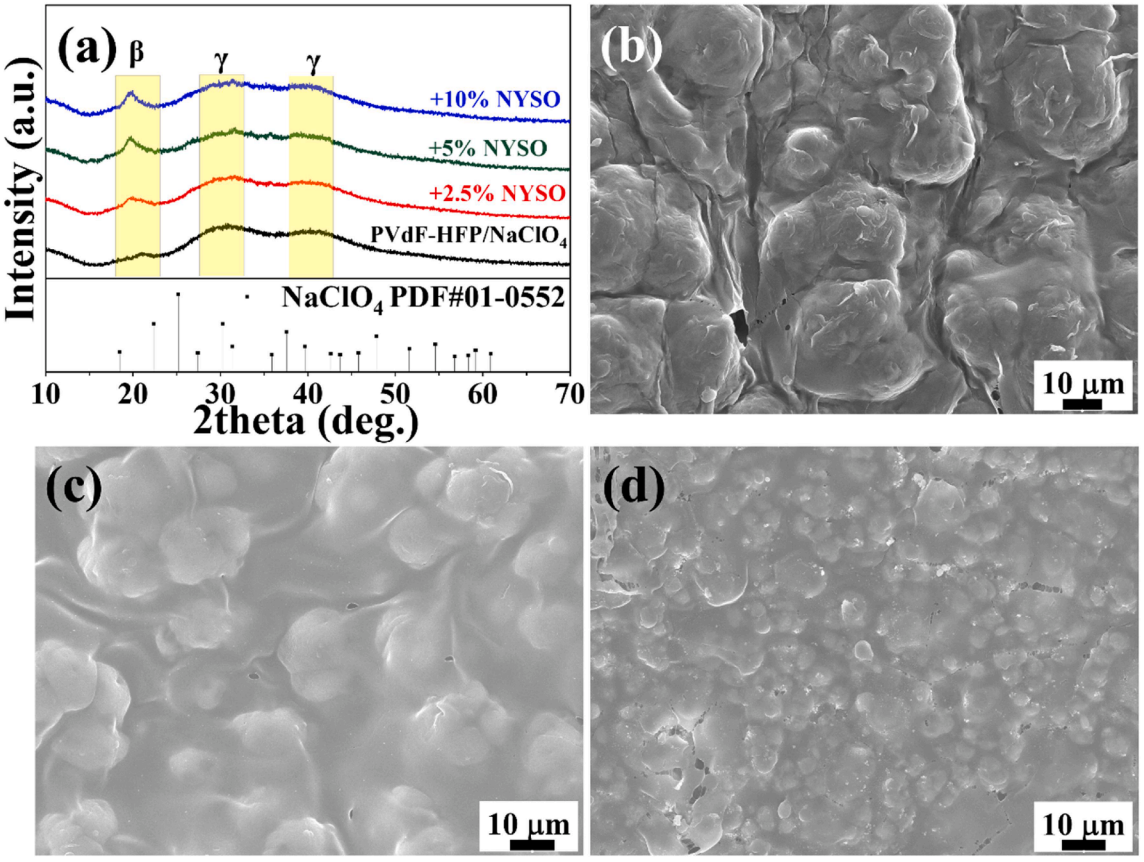

Fig. 1. (a) XRD patterns of free-standing membranes, and SEM images of free-standing membranes containing (b) 2.5 %, (c) 5 %, and (d) 10 % NYSO filler.

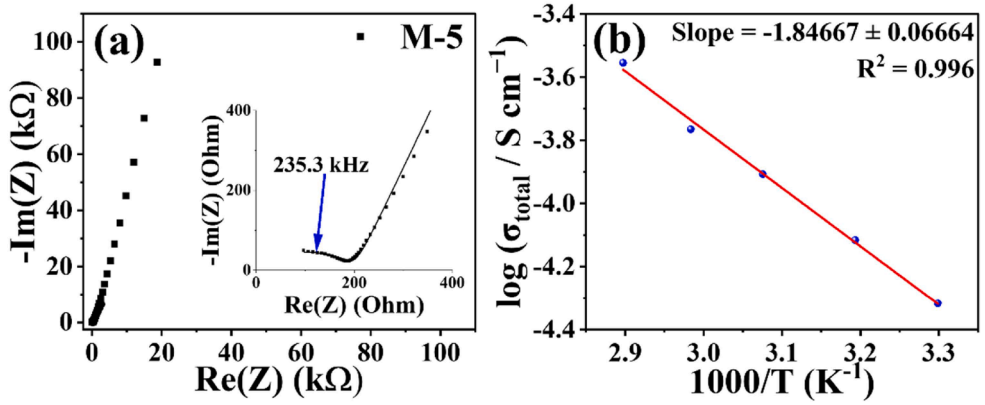

Fig. 2. (a) EIS measurements of M-5 between two blocking electrodes, and (b) the Arrhenius plot of M-5 at different temperatures.

3.2. Characterization of the composite coating layer

Optimized NYSO filler ratios were evaluated in PVdF-HFP/$NaClO_4$ membranes (Fig. 1a). XRD confirmed β/γ-phase dominance in PVdF-HFP, with enhanced β-phase at higher NYSO loadings (2.5–10 %) due to filler-polymer interactions [22,23]. $NaClO_4$ peaks were absent, indicating salt-polymer compatibility. The XRD patterns of NYSO filler did not show clear peaks due to their small particle size and low content, which led to peak broadening and reduced diffraction intensity. Additionally, nanoscale materials may have more structural disorder or strain, further contributing to peak broadening and reduced clarity in the XRD pattern [24].

At low filler loadings (2.5 % and 5 %, Fig. 1b and c), the membranes retain a relatively smooth surface morphology like the pristine NYSO-free membrane (Fig. S5), with uniformly dispersed NYSO particles and minimal agglomeration, suggesting effective integration of the filler within the polymer matrix [23]. However, at 10 % NYSO (Fig. 1d), surface morphology was different from others, implying that aggregation of filler occurred [24].

EIS analysis (Figs. 2a and S6) revealed the 5 % NYSO-loaded membrane (M-5) showed highest ionic conductivity (4.6×10^{-5} S cm^{-1}). The Arrhenius plot (Fig. 2b) demonstrated low activation energy (0.37 eV) for M-5, indicating efficient ion transport [22,25]. These results demonstrate M-5 is the optimal choice for HC particle coating to enhance electrode-electrolyte interfaces.

XRD analysis of b-HC (Fig. 3a) showed two broad peaks at 23.7° (002) and 43.3° (100), characteristic of disordered carbon [26,27]. The c-HC pattern revealed no additional peaks. SEM images (Fig. 3b and c)

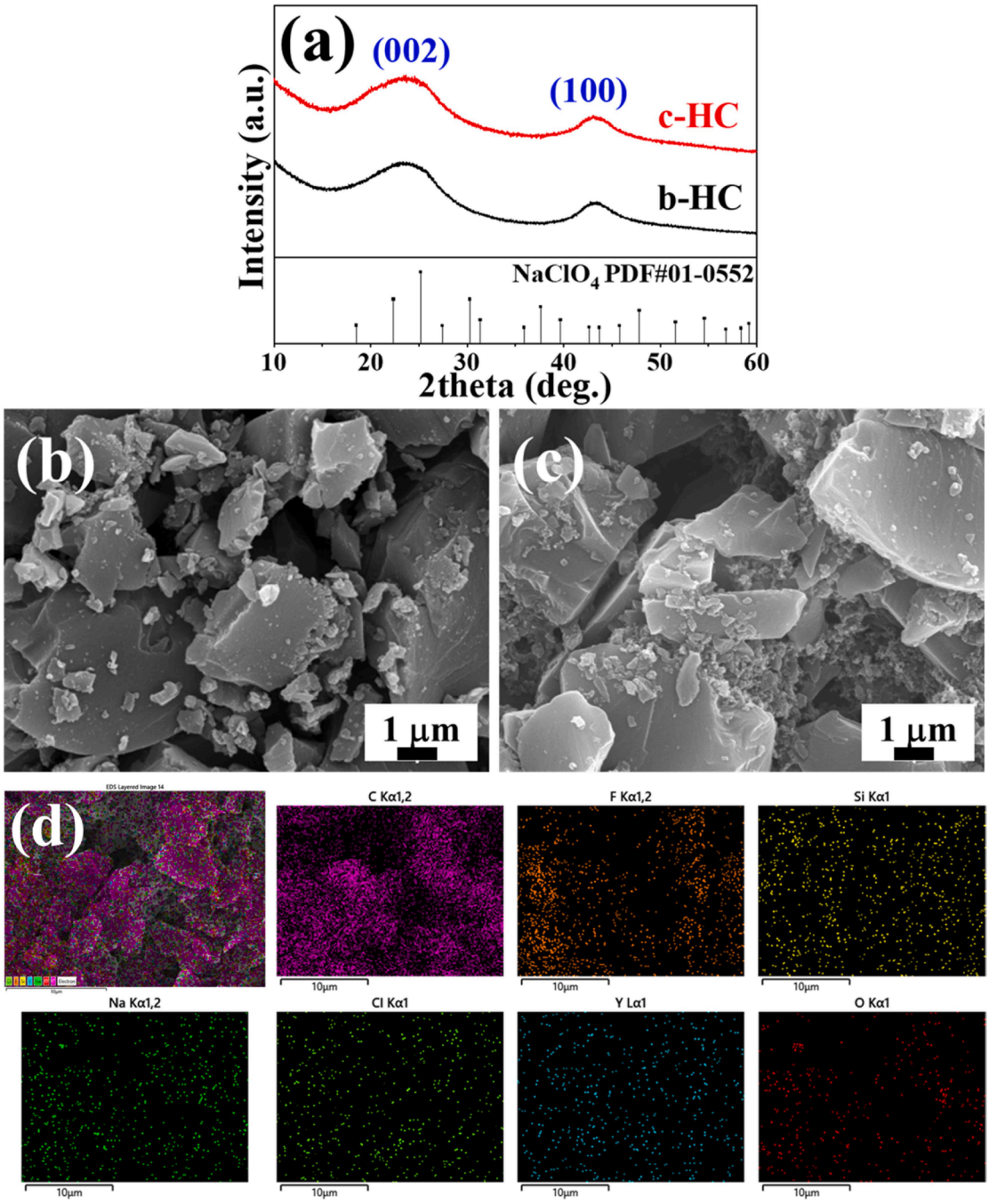

Fig. 3. (a) XRD patterns of b-HC and c-HC; SEM images of (b) b-HC and (c) c-HC; (d) Elemental distribution map of c-HC obtained from EDX analysis.

confirmed the coating preserved b-HC's rough morphology while forming a polymer network between particles, enhancing mechanical and ionic properties [28,29].

EDX mapping (Figs. 3d and S7–S9) confirmed pure carbon composition of b-HC, while c-HC exhibited uniform distribution of F (PVdF-HFP), Cl ($NaClO_4$), and Si (NYSO), indicating NYSO/PVdF-HFP was successfully coated on HC [28–30]. XPS (Fig. S10) further validated the coating layer, with peaks corresponding to PVdF-HFP (F 1*s*), $NaClO_4$ (Na 2*s*/2*p*), NYSO (Si 2*s*, Y $3p_3$, O *1s*), and carbon substrate (C 1*s*) [22,30].

TEM analysis was performed to elucidate the structural features of the coated hard carbon particles, as illustrated in Fig. 4. Fig. 4(a) demonstrates a uniform coating layer enveloping the hard carbon particle, with an estimated thickness of approximately 5–8 nm, as shown inset of Fig. 4a. High-resolution TEM (HRTEM) observation in Fig. 4(b) reveals the presence of crystalline domains within the coating layer, characterized by a lattice spacing of 0.28 nm. This lattice spacing corresponds to the (440) plane of NYSO, confirming the successful incorporation of the NYSO filler into the coating matrix.

3.3. Electrochemical performance and kinetic analysis

Fig. 5 presents the electrochemical performance of c-HC coated with M-5. The c-HC voltage profiles at varying rates (Fig. 5a) mirror those of b-HC (Fig. S11a), suggesting the coating does not alter sodium storage mechanisms. The ICE improved from 85 % of b-HC to 89 % of c-HC at 0.02 A g^{-1}, reflecting the positive effect of composite coating layer [22, 31]. The composite coating functioned as an artificial pre-SEI layer, significantly suppressing electrolyte decomposition and the formation of

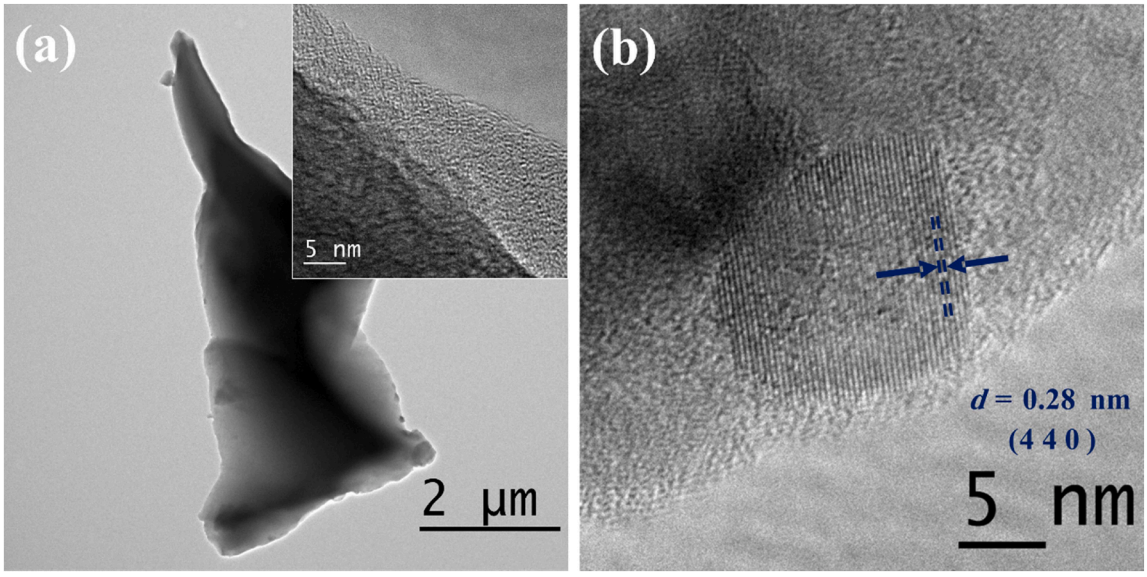

Fig. 4. (a) TEM image of a coated hard carbon particle; inset shows a 5 ~ 8 nm thick coating layer, (b) HR-TEM image revealing lattice fringes of NYSO.

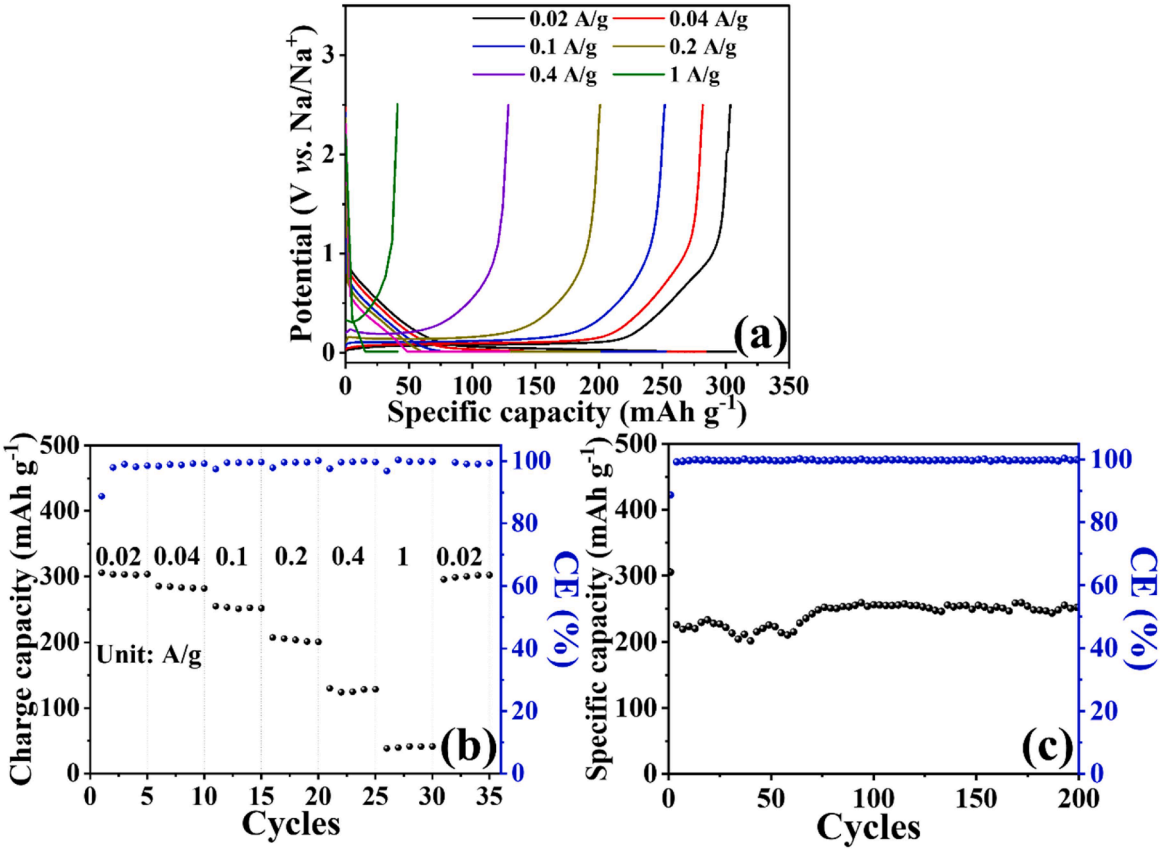

Fig. 5. (a) Voltage profiles of c-HC at various current densities, (b) rate performance of c-HC, and (c) cycling stability at 200 mA g^{-1}.

a conventional SEI [31].

The corresponding C-rate performance is illustrated in Figs. 5b and S11b. The delivered capacities of c-HC are comparable to b-HC, benefiting from high ionic conductivity of composite coating layer [11]. Figs. 5c and S11c present the cycling stability of c-HC and b-HC at a current rate of 200 mA g^{-1}. The data indicate that c-HC exhibits superior long-term stability compared to b-HC. Over repeated cycling, c-HC maintains a higher capacity, whereas b-HC undergoes more significant capacity fading, particularly after ~ 90 cycles.

The enhanced cycling performance of c-HC is attributed to the protective coating, which likely mitigates electrolyte decomposition and prevents excessive structural degradation [32]. This coating may act as a barrier against undesirable side reactions at the electrode/electrolyte interface, thereby improving the long-term stability of the material [33]. Additionally, the coating layer helps preserve the integrity of the electrode, reducing mechanical stress and capacity loss over prolonged

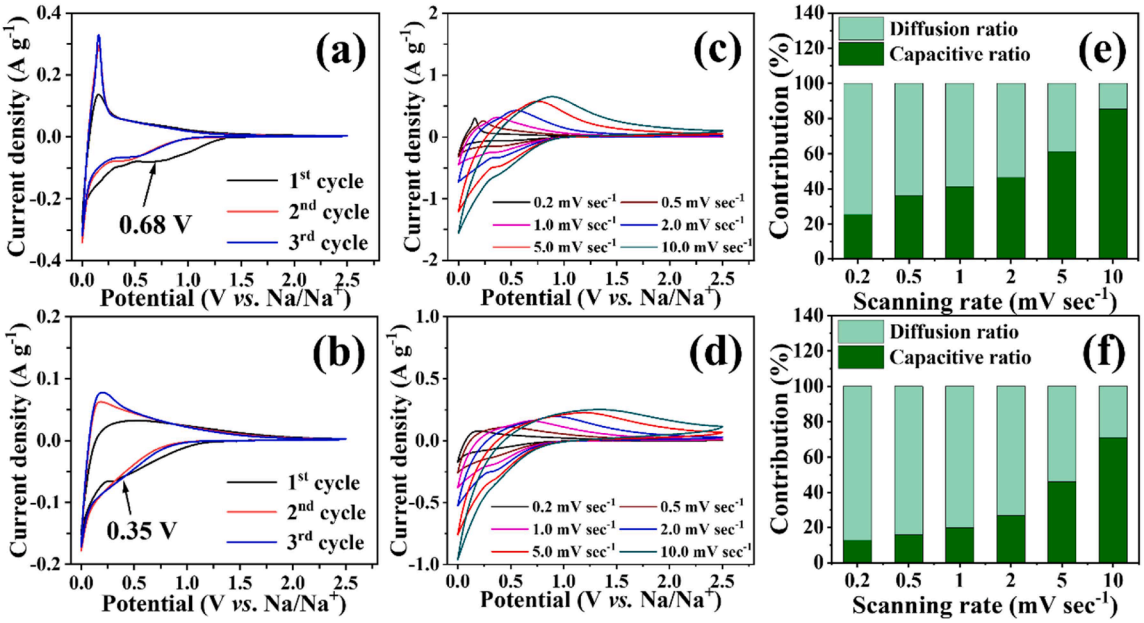

Fig. 6. Electrochemical performance analysis: (a, b) Initial three cyclic voltammograms recorded at a scan rate of 0.2 mV sec^{-1}; (c, d) Cyclic voltammograms at varying scan rates; and (e, f) Contribution of diffusion-controlled and capacitive processes for b-HC and c-HC, respectively.

cycling [34]. In contrast, b-HC suffers from more rapid capacity decay as shown in Fig. S11c, suggesting increased reactivity with the electrolyte and possible structural instability over extended cycling [11].

The CV analysis of b-HC and c-HC (Fig. 6a and b) revealed similar redox peaks (0 ~ 0.25 V) for Na-ion storage, confirming unchanged adsorption/intercalation mechanisms [28,35]. b-HC showed a prominent SEI formation peak at 0.68 V in the first cycle, indicating irreversible Na trapping that stabilized in later cycles [9,28]. In contrast, c-HC shifted SEI formation to 0.35 V, demonstrating suppressed side reactions and higher ICE due to the coating [36]. Both materials exhibiting Na-ion extraction at 0.16 V that the composite coating effectively suppresses irreversible side reactions and SEI formation, thereby improving the ICE [37].

CV measurements at various scan rates (Fig. 6c and d) showed significant polarization between sodium insertion (reduction) and extraction (oxidation) peaks, with the oxidation peak for c-HC appearing at higher voltage than b-HC, indicating increased extraction overpotential. The more intense reduction peak suggests easier Na^+ insertion compared to the kinetically hindered extraction process in c-HC [16]. Kinetic analysis (Fig. 6e and f) revealed c-HC's greater diffusion-controlled contribution, attributed to the coating layer's ability to improve ion diffusion. The composite coating may modify electrode porosity and surface characteristics, create more accessible sites while potentially introducing pseudocapacitive storage behavior that enhances diffusion kinetics.

Analysis of CV peak currents (Fig. S12) revealed b-HC exhibited higher Na^+ diffusion coefficients than c-HC for both reductions (1.8×10^{-8} *vs.* 6.4×10^{-9} cm^2 s^{-1}) and oxidation (1.5×10^{-9} *vs.* 2.8×10^{-10} cm^2 s^{-1}) processes (Table S1). The significantly lower Na^+ diffusion coefficients for c-HC confirm that the coating introduced kinetic barriers to solid-state ion transport [9,22,38]. While such barriers could limit rate capability, they would simultaneously enhance interfacial stability by suppressing parasitic reactions [9,22]. Notably, c-HC exhibits a higher relative contribution from diffusion-controlled storage (Fig. 6e and f). This suggests that the coating preferentially suppresses competing capacitive processes or modifies interfacial properties. Further optimization of coating parameters should target this critical trade-off, particularly for high-rate full-cell operation [38].

The interfacial stability of b-HC and c-HC were investigated using EIS as displayed in Fig. 7(a and b). Fresh b-HC had an R_{ct} of 65.4 Ω

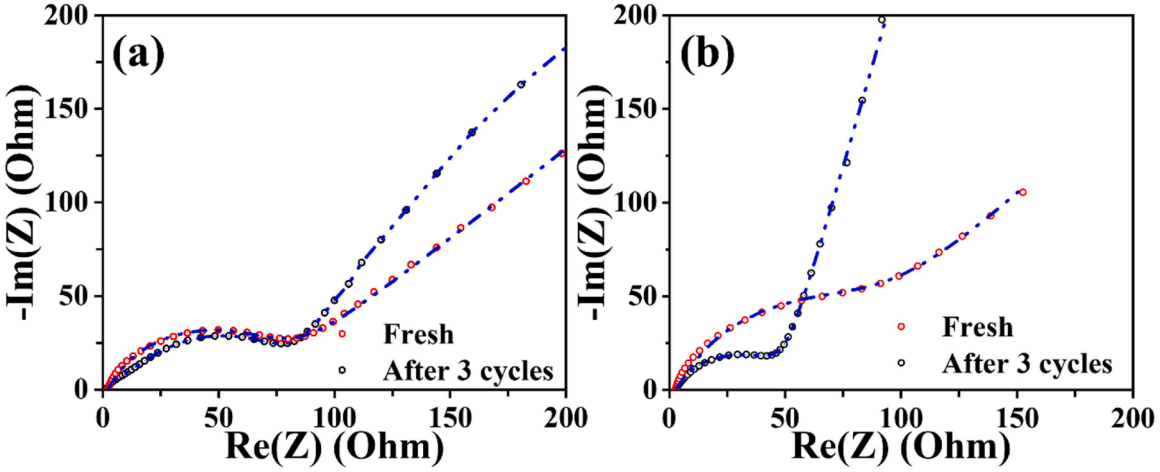

Fig. 7. EIS spectra of (a) b-HC and (b) c-HC before and after 3 cycles.

(Table S2), while c-HC showed higher initial R_{ct} (84.6 Ω). This initially higher R_{ct} observed in c-HC can be attributed to the physical presence of the NYSO-polymer composite coating. While the coating is ionically conductive, it may slightly reduce the effective active surface area for charge transfer and introduce minor kinetic resistance to Na^+ transport across the interface [39]. Given that sodium ion storage primarily involves adsorption and pore filling, the coating can hinder access to active sites, thereby increasing the initial R_{ct} [2,3]. However, this initial high impedance is a necessary trade-off for the substantial long-term benefits provided by the coating [39].

After cycling, b-HC exhibited significant R_{SEI} (18.8 Ω), confirming SEI growth that reduced ICE. R_{ct} of b-HC decreased to 53.2 Ω, but total resistance (R_t) rose to 73.5 Ω due to SEI effects [40,41]. In contrast, cycled c-HC displayed no R_{SEI} (Table S2) and a sharp R_{ct} drop to 45.4 Ω, indicating the coating enhanced the interfacial resistance. This yielded lower R_t (48.3 Ω) *versus* b-HC (73.5 Ω), demonstrating dual benefits: interface stabilization and faster charge transfer [40]. The absence of R_{SEI} and lower R_{ct} in c-HC align with its superior ICE and cycling stability [29,40]. These results confirm the coating's effectiveness for practical sodium-ion batteries [31,41].

4. Conclusions

The $Na_5YSi_4O_{12}$ (NYSO)-based composite coating significantly improves hard carbon anode performance by enhancing initial Coulombic efficiency and cycling stability, particularly at high rates (200 mA g^{-1}). Characterizations confirmed the coating modifies the electrode-electrolyte interface, reducing charge transfer resistance while increasing diffusion-controlled sodium storage contributions. By mitigating initial capacity fading and maintaining favorable Na^+ transport kinetics, the coating demonstrates dual functionality in interface stabilization and ion transport enhancement. These findings establish the NYSO-based composite coating as a promising approach for optimizing hard carbon anodes. Further enhancement of the electrode performance is expected through coating parameter optimization.

CRediT authorship contribution statement

Mohamed M. Abdelaal: Writing – original draft, Investigation, Formal analysis. **Pandeeswari Jayaraman:** Investigation, Formal analysis. **Kei Nishikawa:** Formal analysis. **Masashi Kotobuki:** Writing – review & editing, Validation, Supervision, Methodology, Funding acquisition, Conceptualization.

Declaration of competing interest

The authors declare that they have no known competing financial interests or personal relationships that could have appeared to influence the work reported in this paper.

Acknowledgements

This research was funded by the Industry-Academic cooperation project (Project title: MCUT and Formosa Smart Energy Tech. Corp., project number: I0-113-S028) and Chang Gung University (URRPD2N0021).

Supplementary materials

Supplementary material associated with this article can be found, in the online version, at doi:10.1016/j.jtice.2025.106329.

Data availability

Data will be made available on request.

References

[1] Kotobuki M, Yan B, Lu L. Recent progress on cathode materials for rechargeable magnesium batteries. Energy Storage Mater 2023;54:227–53.
[2] Tan S, Yang H, Zhang Z, Xu X, Xu Y, Zhou J, Zhou X, Pan Z, Rao X, Gu Y, Wang Z, Wu Y, Liu X, Zhang Y. The Progress of Hard Carbon as an Anode Material in Sodium-Ion Batteries. Molecules 2023;28(7):3134.
[3] Wu C, Yang Y, Zhang Y, Xu H, He X, Wu X, Chou S. Hard carbon for sodium-ion batteries: progress, strategies and future perspective. Chem Sci 2024;15(17):6244–68.
[4] Abdelaal MM, Hsu H-H, Liao W-L, Mohamed SG, Yang C-C, Hung T-F. Hierarchical porous activated carbon anode for dual carbon lithium-ion capacitors: energy storage mechanisms and electrochemical performances. J Taiwan Inst Chem Eng 2024;154:104912.
[5] Sun N, Qiu J, Xu B. Understanding of sodium storage mechanism in hard carbons: ongoing development under debate. Adv Energy Mater 2022;12(27):2200715.
[6] Asfaw HD, Tai CW, Valvo M, Younesi R. Facile synthesis of hard carbon microspheres from polyphenols for sodium-ion batteries: insight into local structure and interfacial kinetics. Mater Today Energy 2020;18:100505.
[7] Li X, Ding C, Liang Q, Hu J, Xu L, Li Y, Liu Y, Gao Y. Progress in hard carbons for sodium-ion batteries: microstructure, sodium storage mechanism and initial Coulombic efficiency. J Energy Storage 2024;98:112986.
[8] Qin N, Sun Y, Hu C, Liu S, Luo Z, Cao X, Liang S, Fang G. Boosting high initial coulombic efficiency of hard carbon by in-situ electrochemical presodiation. J Energy Chem 2023;77:310–6.
[9] Liu Z-T, Hsu Y-C, Chien S-C, Liu W-R. Temperature effects on lithium/sodium-ion storage behaviors of hard carbon microspheres derived from phenolic resin as potential anode for rechargeable batteries applications. J Taiwan Inst Chem Eng 2024;164:105698.
[10] Chen F, Di Y, Su Q, Xu D, Zhang Y, Zhou S, Liang S, Cao X, Pan A. Vanadium-modified hard carbon spheres with sufficient pseudographitic domains as high-performance anode for sodium-ion batteries. Carbon Energy 2023;5(2):e191.
[11] Wang B, Li Y, Yuan F, Sun Q, Li Z, Zhang D, Sun H, Wang Q, Zhang W, Wang W. Conductive layer coupled mesoporous hard carbon enabling high rate and initial Coulombic efficiency for potassium ion battery. Chem Eng J 2024;494:153081.
[12] Abdelaal MM, Wang Z, Shen H, Pan Z, Kotobuki M. Electrochemical properties of a La-doped $Na_5YSi_4O_{12}$ ceramic electrolyte. ACS Appl Energy Mater 2025;8:9656–62.
[13] Wang Y, Wang Z, Zheng F, Sun J, Oh JAS, Wu T, Chen G, Huang Q, Kotobuki M, Zeng K, Lu L. Ferroelectric Engineered Electrode-Composite Polymer Electrolyte Interfaces for All-Solid-State Sodium Metal Battery. Adv Sci 2022;9(13):2105849. M. Kotobuki, L. Lu, S.V. Savilov, S.M. Aldoshin, J. Electrochem. Soc. 164(14) (2017) A3868-A3875.
[14] Jayaraman P, Abdelaal MM, Chien W-C, Moriya M, Kotobuki M. Development of a novel gel-polymer electrolyte based on PVDF-HFP polymer and triethylammonium Chloride (TEMACl) for room-temperarture chloride-ion batteries. Electrochim Acta 2025;537:146808.
[15] Abdelaal MM, Yang C-C, Hung T-F. Electrochemical performances and Li^+-storage mechanism of highly proportional 1T-MoS_2/hierarchical porous activated carbon nanocomposites. J Energy Storage 2024;77:109926.
[16] Amirtha RM, Chang S-M, Abdelaal MM, Yang C-C, Hung T-F. Efficient zinc protection enabled by polyhedral metal-organic framework and ionic-crosslinking binder. Electrochim Acta 2024;496:144526.
[17] Okura T, Yoshida N, Yamashita K. Na^+ superionic conducting silicophosphate glass-ceramics – review. Solid State Ion 2016;285:143–54.
[18] Liu L, Xu Y, Zhou X, Guo W, Li J, Guo X, Jiang Y. Conductivity behavior of $Na_5YSi_4O_{12}$ and its typical structural analogues by solution-assisted solid-state reaction for solid-state sodium battery. J Solid State Chem 2024;336:124781.
[19] Kotobuki M, Yanagiya S. Li-ion conductivity of NASICON-type $Li_{1+2x}Zr_{2-x}Ca_x(PO_4)_3$ solid electrolyte prepared by spark plasma sintering. J Alloy Compd 2021;862:158641.
[20] Hüttl J, Cai W, Wagner D, Schilm J, Kusnezoff M, Nikolowski K, Shaji N, Lee CW, Partsch M, Michaelis A. Polarization impedance at the Na-$Na_5YSi_4O_{12}$ interface. Solid State Ion 2022;376:115856.
[21] Gunamony J, Walle KZ, Kotobuki M. Influence of mixing technique on properties of $Li_{1.3}Al_{0.3}Ti_{1.7}(PO_4)_3$ solid electrolyte prepared by the solid-state reaction-A comparison of dry 3D mixing technique with wet ball-milling. Solid State Ion 2024;410:116528.
[22] Shu K, Zhou J, Wu X, Liu X, Sun L, Wang Y, Tian S, Niu H, Duan Y, Hu G, Wang H. A PVDF/g−C_3N_4-based composite polymer electrolytes for sodium-ion battery. Polym (Basel) 2023;15(9):2006.
[23] Xu Y-S, Kuan W-F. Asymmetrically architectured PVDF membranes with enhanced ion conduction for lithium-metal battery. J Taiwan Inst Chem Eng 2024;158:104910.
[24] Holder CF, Schaak RE. Tutorial on powder X-ray diffraction for characterizing nanoscale materials. ACS Nano 2019;13(7):7359–65.
[25] M. J KK, Kalathi JT. Investigation on the dielectric performance of PVDF-HFP/LZO composites. J Alloy Compd 2020;843:155889.
[26] Abdelaal MM, Hung T-C, Mohamed SG, Yang C-C, Huang H-P, Hung T-F. A comparative study of the influence of nitrogen content and structural characteristics of NiS/nitrogen-doped carbon nanocomposites on capacitive performances in alkaline medium. Nanomaterials 2021;11(7):1867.
[27] Abdelaal MM, Hung T-C, Mohamed SG, Yang C-C, Hung T-F. Two birds with one stone: hydrogel-derived hierarchical porous activated carbon toward the capacitive performance for symmetric supercapacitors and lithium-ion capacitors. ACS Sustain Chem Eng 2022;10(14):4717–27.

[28] Liu Z-T, Hsieh T-H, Huang C-W, Lee M-L, Liu W-R. Temperature effects on hard carbon derived from sawdust as anode materials for sodium ion batteries. J Taiwan Inst Chem Eng 2024;154:104889.
[29] Amirtha RM, Hsu H-H, Abdelaal MM, Anbunathan A, Mohamed SG, Yang C-C, Hung T-F. Constructing a carbon-encapsulated carbon composite material with hierarchically porous architectures for efficient capacitive storage in organic supercapacitors. Int J Mol Sci 2022;23(12):6774.
[30] Wang C-C, Su W-L. Ultrathin artificial solid electrolyte interface layer-coated biomass-derived hard carbon as an anode for sodium-ion batteries. ACS Appl Energy Mater 2022;5(1):1052–64.
[31] Zhao S, Huang F. Weakly solvating few-layer-carbon interface toward high initial coulombic efficiency and cyclability hard carbon anodes. ACS Nano 2024;18(2):1733–43.
[32] He X-X, Zhao J-H, Lai W-H, Li R, Yang Z, Xu C-m, Dai Y, Gao Y, Liu X-H, Li L, Xu G, Qiao Y, Chou S-L, Wu M. Soft-carbon-coated, free-standing, low-defect, hard-carbon anode to achieve a 94% initial coulombic efficiency for sodium-ion batteries. ACS Appl Mater Interfaces 2021;13(37):44358–68.
[33] Fan X, Kong X, Zhang P, Wang J. Research progress on hard carbon materials in advanced sodium-ion batteries. Energy Storage Mater 2024;69:103386.
[34] Li N, Zhao J, Long Z, Song R, Cui Y, Lin J, Xu H, Huang Y. Metalized plastic current collectors incorporated with halloysite nanotubes toward highly safe lithium-ion batteries. Adv Funct Mater 2024;34(32):2316582.
[35] Cheng D, Zhou X, Hu H, Li Z, Chen J, Miao L, Ye X, Zhang H. Electrochemical storage mechanism of sodium in carbon materials: a study from soft carbon to hard carbon. Carbon N Y 2021;182:758–69.
[36] Palanisamy K, Daboss S, Schäfer D, Rohnke M, Derr L, Lang M, Schuster R, Kranz C. Spray-coated hard carbon composite anodes for sodium-ion insertion. Batter Supercaps 2024;7(1):e202300402.
[37] Wang F, Jiang Z, Zhang Y, Zhang Y, Li J, Wang H, Jiang Y, Xing G, Liu H, Tang Y. Revitalizing sodium-ion batteries via controllable microstructures and advanced electrolytes for hard carbon. eScience 2024;4(3):100181.
[38] Gong Y, Yu C, Li Y, Qian J, Wu C, Bai Y. Constructing robust solid electrolyte interface via ZrO_2 coating layer for hard carbon anode in sodium-ion batteries. Batteries 2022;8(9):115.
[39] Fedorova AA, Levin OV, Eliseeva SN, Katrašnik T, Anishchenko DV. Investigating the coating effect on charge transfer mechanisms in composite electrodes for lithium-ion batteries. Int J Mol Sci 2023;24(11):9406.
[40] Beda A, Zallouz S, Hajjar-Garreau S, El Marouazi H, Simonin L, Ghimbeu CM. Impact of Na-carboxymethyl cellulose binder type on hard carbon performance and SEI formation in sodium-ion batteries. ACS Appl Mater Interface 2024;16(49):68664–79.
[41] Liao W-L, Hung T-F, Abdelaal MM, Chao C-H, Fang C-C, Mohamed SG, Yang C-C. Highly efficient sodium-ion capacitor enabled by mesoporous $NaTi_2(PO_4)_3$/C anode and hydrogel-derived hierarchical porous activated carbon cathode. J Energy Storage 2022;55:105719.